Real-time study of *a*-Si:H/*c*-Si heterointerface formation and epitaxial Si growth by spectroscopic ellipsometry, infrared spectroscopy, and second-harmonic generation

J. J. H. Gielis, P. J. van den Oever, B. Hoex, M. C. M. van de Sanden, and W. M. M. Kessels*
Department of Applied Physics, Eindhoven University of Technology, P.O. Box 513, 5600 MB Eindhoven, The Netherlands
(Received 7 December 2007; revised manuscript received 27 March 2008; published 29 May 2008)

The performance of many devices based on Si thin films deposited on crystalline Si (*c*-Si) is highly governed by interface quality. For many of these applications, only fully epitaxial films or fully amorphous films having an abrupt interface with the substrate are desired. However, the realization of these perfectly sharp interfaces and the mechanisms governing their formation are not fully understood yet. In this study, the interface formation between Si thin films and *c*-Si has been investigated by simultaneously applying three complementary optical techniques in real time during low temperature Si film growth. The films were deposited in a hot-wire chemical vapor deposition process by using both native oxide covered and H terminated Si(100) substrates. The formation of hydrogenated amorphous Si (*a*-Si:H), epitaxial Si, and mixed phase Si has been detected with spectroscopic ellipsometry by measuring the optical properties of the growing films. The evolution of the hydrogen content and hydrogen bonding configurations in the films has been monitored by attenuated total reflection infrared spectroscopy. A clear dependence of the hydrogen content on film morphology is observed with the amorphous films containing significantly more hydrogen. The surface and interface sensitive technique of second-harmonic generation (SHG) has been applied both spectroscopically and in real time. The SHG spectra of *a*-Si:H films on Si(100) obtained in the SHG photon energy range of 2.7–3.5 eV revealed a dominant contribution originating from the film/substrate interface related to E_0'/E_1 critical point (CP) transitions of *c*-Si. The real-time behavior of the SHG response is shown to strongly depend on differences in initial film morphology, which allows for identification of direct *a*-Si:H/*c*-Si heterointerface formation, nanometer-level epitaxial growth, and fully epitaxial growth at a very early stage of film growth. On the basis of the results obtained by the three optical techniques, the *c*-Si surface passivation mechanism by *a*-Si:H thin films is addressed and it is demonstrated that the combination of the techniques provides a profound method to control processes occurring during Si thin film growth.

DOI: 10.1103/PhysRevB.77.205329 PACS number(s): 78.66.−w, 42.65.Ky, 78.68.+m, 81.15.Gh

I. INTRODUCTION

Amorphous and epitaxial silicon thin films deposited on wafer-type substrates are currently attracting considerable attention in photovoltaics and microelectronics. Silicon heterojunction (SHJ) solar cells based on the heterojunction between ultrathin hydrogenated amorphous silicon (*a*-Si:H) films (~50 Å) and crystalline silicon (*c*-Si) have been reported to reach efficiencies as high as 22.3%.[1,2] Ultrathin *a*-Si:H films yield an excellent passivation of *c*-Si surfaces and are, for example, applied in diffused emitter *c*-Si solar cells for rear surface passivation[3] and in thin film polysilicon solar cells by using a heterojunction emitter.[4] Recently, *a*-Si:H has also been proven to be successful to passivate germanium surfaces, illustrating the potential of *a*-Si:H to increase the efficiency of germanium photovoltaic cells.[5] The low temperature growth of epitaxial silicon (epi-Si) is a promising method to thicken *c*-Si seed layers on low-cost substrates for solar cell concepts based on thin film *c*-Si and also to add Si layers to wafers without disturbing doping profiles.[6,7] In Ge and GaAs based high mobility metal-oxide-semiconductor field-effect transistors, the application of ultrathin amorphous and epitaxial silicon interface passivation layers has been shown to improve high-κ gate stack performance.[8,9]

The performance of these thin film based devices in the aforementioned examples is highly determined by interface quality. For high-performance SHJ solar cells and well passivated surfaces, it is essential to form an abrupt and atomically flat interface between *a*-Si:H and *c*-Si without any nanometer-level epitaxial growth.[10,11] In case of Si epitaxy, a layer of perfectly crystalline Si is required, while the formation of any polycrystalline or amorphous material needs to be suppressed to avoid epitaxial breakdown.[7]

The morphology of a Si film is influenced by several factors, such as the deposition temperature, the nature of the substrate surface, the growth rate, the surface roughness, and the hydrogen content of the developing film.[6,11–13] These factors might result in conflicting processing conditions. For example, at lower substrate temperatures, *a*-Si:H films are obtained, while at higher temperatures, epi-Si tends to develop.[12] However, the *a*-Si:H film properties improve with increasing temperature, such that the highest solar cell efficiencies are obtained at temperatures close to the transition to epi-Si, consequently enhancing the chance of nanometer-level epitaxial material formation.[13] This effect is illustrated in Fig. 1 where the surface recombination velocity at the *a*-Si:H/*c*-Si interface is shown as a function of the film deposition temperature. Every data point in Fig. 1 represents a different H terminated Si(100) sample with films deposited on both sides (details about the deposition are described in Sec. III). The surface recombination velocity is a measure for surface passivation and is deduced from carrier lifetime spectroscopy.[14,15] With increasing deposition temperature, the surface passivation significantly improves up to ~140 °C, indicating an improvement of the properties of the

 ©2008 The American Physical Society

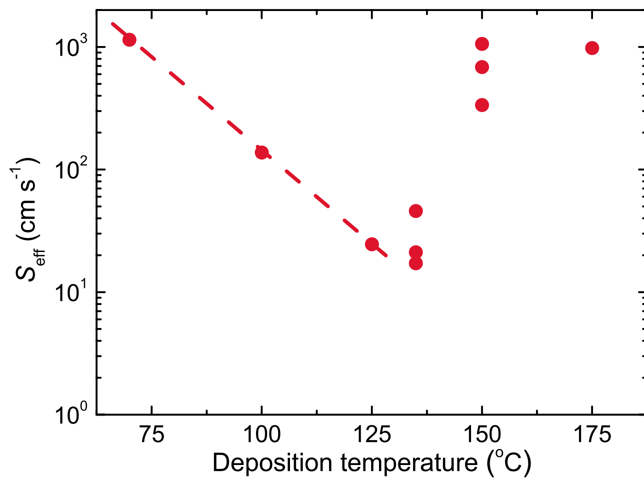

FIG. 1. (Color online) Surface recombination velocity as a function of Si film deposition temperature. Every data point represents a different sample. The suggested improvement of passivation properties with increasing deposition temperatures until ~140 °C where the passivation properties abruptly deteriorate is indicated by the dashed line that serves as a guide to the eye. The films, having a thickness of 150–300 Å, were deposited on both sides of H terminated Si(100) substrates by using sample treatment B. Except for the deposition temperature, the experimental conditions were kept constant for all films.

a-Si:H and the *a*-Si:H/*c*-Si interface. For temperatures above ~140 °C, the surface passivation abruptly deteriorates, which is caused by the formation of epitaxial material during the initial film growth. Although parameters such as the deposition temperature, the substrate condition, and the growth rate are known to have an impact on Si film structure, the underlying mechanism governing whether a film develops purely epitaxial or entirely amorphous with a sharp interface is not fully understood yet.

The formation of Si thin films has been studied by several authors by using *ex situ* techniques such as transmission electron microscopy (TEM)[6,10,16,17] and secondary ion mass spectrometry (SIMS).[12,16,17] Also carrier lifetime spectroscopy, as discussed above, has proven to be a useful diagnostic to measure the abruptness of *a*-Si:H/*c*-Si interfaces.[15,16] Although providing detailed information on film structure and composition, these *ex situ* methods do not provide fast process feedback and information on the real-time evolution of the film properties. Moreover, TEM and SIMS are sample destructive. For detailed fundamental understanding of the growth mechanism as well as for process monitoring, *in situ* techniques that are applicable in real time during film growth are desired. For example, time-resolved microwave conductivity is a technique that has been used to study *a*-Si:H film growth *in situ*.[18] In particular, all-optical techniques are very useful for *in situ* applications due to their noninvasive nature and real-time applicability. The formation of both amorphous and epitaxial films on *c*-Si has been studied *in situ* by using spectroscopic ellipsometry (SE),[7,12,13,19–25] whereas amorphous film growth on *c*-Si has been investigated with attenuated total reflection Fourier transform infrared spectroscopy (ATR-FTIR).[21,22,25] In a recent publication, we reported on the simultaneous application of SE, ATR-FTIR, and SHG during low temperature Si film growth on H terminated Si(100).[26] In this paper, we present an extended set of experimental data obtained with these three techniques and these data are analyzed in a more detailed way. From studies on native oxide covered and H terminated Si(100) substrates, it will be demonstrated that the three optical techniques SE, ATR-FTIR, and SHG provide important complementary information on the morphology development of Si films in terms of critical point resonances and H content. It will also be shown that especially SHG exhibits an excellent sensitivity to initial film morphology providing a distinction between direct heterointerface formation and epitaxial growth.

This paper is organized as follows. In Sec. II, we introduce the optical diagnostics SE, ATR-FTIR, and SHG and we discuss relevant applications of these techniques reported in literature. In Sec. III, the details of the high vacuum reactor, the deposition procedure, the preparation of the Si substrates, and the optical setups for the experiments are discussed. Additionally, we briefly introduce *ex situ* techniques used to complement and validate the results of the optical diagnostics. In Sec. IV, the results obtained by SE, ATR-FTIR, and SHG are presented and analyzed. Finally, in Sec. V, the results and conclusions are summarized.

II. REAL-TIME OPTICAL DIAGNOSTICS

In this section, the optical diagnostics SE, ATR-FTIR, and SHG used to study the growth of Si thin films will be introduced in more detail. We will predominantly focus on SHG, as this is not yet a well-established technique to study Si film growth. The first technique, spectroscopic ellipsometry, measures the change in polarization of light upon reflection from a surface and provides information on linear optical properties, thickness, and surface roughness of films and substrates. Application of SE in real time during processing has provided information on the nucleation, coalescence, growth, and surface roughness evolution of *a*-Si:H thin films.[12,13,19–25] Also, the formation of fully epitaxial Si and the breakdown of epi-Si into mixed phase material have been characterized with real-time SE.[7,12,13] With ATR-FTIR, the absorption of infrared radiation by chemical bonds is measured. Multiple reflections in the ATR crystal enhance the sensitivity of the technique. By probing Si-H stretching vibrations, the bonding of hydrogen can be resolved, both in the bulk and at the surface of the film. The sensitivity to surface Si-H bonds allowed for the identification of the role of SiH_x radicals during *a*-Si:H growth on GaAs substrates,[27,28] whereas the sensitivity to bulk Si-H bonds provided detailed information on the evolution of the H content in *a*-Si:H deposited on *c*-Si.[21,22,25] To our knowledge, ATR-FTIR has not yet been applied to study the formation of epitaxial or mixed phase Si films.

The third diagnostic applied here, which is second-harmonic generation, is a surface and interface sensitive nonlinear optical technique that allows for real-time probing of the interface between the Si films and the *c*-Si substrates. Microscopically, SHG is the conversion of two photons with energy $\hbar\omega$ into a single photon with energy $2\hbar\omega$. SHG occurs when incident radiation with a fundamental photon en-

ergy $\hbar\omega$ and an electric field $\mathbf{E}(\omega)$ induces a second-order nonlinear polarization $\mathbf{P}^{(2)}(2\omega)$ in a medium that, as a result, radiates at twice the fundamental frequency. Within the electric dipole approximation, SHG is described by[29]

$$\mathbf{P}^{(2)}(2\omega) = \varepsilon_0 \overleftrightarrow{\chi}^{(2)}(2\omega):\mathbf{E}(\omega)\mathbf{E}(\omega), \tag{1}$$

where $\overleftrightarrow{\chi}^{(2)}(2\omega)$ is the second-order nonlinear susceptibility tensor being a material property. The sensitivity of the technique to surfaces and interfaces arises from the fact that SHG is forbidden in the bulk of centrosymmetric media, such as *c*-Si and *a*-Si:H. For these materials, symmetry considerations imply $\overleftrightarrow{\chi}^{(2)}=0$, whereas at a surface or interface, the symmetry is broken and as a result $\overleftrightarrow{\chi}^{(2)}$ is nonzero. For SiO_2/Si(100) interfaces, Si(100) surfaces, as well as surfaces and interfaces of amorphous media such as *a*-Si:H, only five components of the second-order nonlinear susceptibility tensor are nonzero, of which only three components are independent. These nonzero components are $\chi^{(2)}_{zzz}$, $\chi^{(2)}_{zxx}=\chi^{(2)}_{zyy}$, and $\chi^{(2)}_{xxz}=\chi^{(2)}_{yyz}$, where x and y define the surface or interface plane with z orthogonal to this plane.[30,31] The process of SHG is resonantly enhanced when the photon energy of either the fundamental or the SHG radiation coincides with the energy of an optical transition in the medium. This aspect makes SHG a powerful technique to probe electronic states at surfaces and buried interfaces of thin films.

SHG has been extensively applied to study clean and H terminated *c*-Si surfaces and SiO_2/*c*-Si interfaces.[32] From controlled H dosing experiments of clean *c*-Si surfaces, SHG has been shown to be sensitive to surface Si dangling bonds in the fundamental photon energy range of $\sim$1.0 to $\sim$1.3 eV.[33–35] Furthermore, characteristic two-photon resonances close to 3.4 eV have been observed at *c*-Si surfaces and buried interfaces. These resonances, being close to the E_0'/E_1 CP transitions of bulk *c*-Si,[36] were suggested to be related to Si-Si bonds distorted or strained due to the presence of a surface or interface[37] and also suggested to be related to the presence of dc electric fields, which leads to electric-field-induced second-harmonic generation (EFISH).[38] These dc electric fields can be generated by surface reconstructions or bulk space-charge regions (SCRs) in the *c*-Si that result from high doping densities, applied bias voltages, and (photon-induced) trapped charge.[39,40] The surface and bulk SCR EFISH polarizations are proportional to the dc electric field $\mathbf{E}_{dc}$,

$$\mathbf{P}^{EFISH}(2\omega) = \varepsilon_0 \overleftrightarrow{\chi}^{(3)}(2\omega):\mathbf{E}(\omega)\mathbf{E}(\omega)\mathbf{E}_{dc}. \tag{2}$$

At higher SHG photon energies, resonances were observed around 4.3 eV, which is near the *c*-Si E_2 CP, and around 3.7 eV. The latter resonance was attributed to Si interband transitions in a thin transition layer between *c*-Si and SiO_2.[41–43]

The characterization of amorphous Si by SHG has remained relatively unexplored. Alexandrova *et al.* performed *ex situ* SHG experiments on *a*-Si:H films deposited on different glass substrates, however, only at a fixed photon energy of 1.17 eV (1064 nm) by using a Nd:yttrium aluminum garnet (YAG) laser.[44] More recently, we reported on both *ex situ* and real-time *in situ* SHG experiments of *a*-Si:H deposited on fused silica substrates investigated by using a Nd:YAG-pumped optical parametric oscillator. In these studies, broad spectral features assigned to both dangling bonds and Si-Si bonds were observed.[31,45] Erley and Daum reported on *ex situ* SHG experiments of a 0.7 μm thick *a*-Si:D film on Si(100) and observed a very weak featureless SHG spectrum that was an order of magnitude lower in intensity than for native oxide covered Si(100).[41] We also reported on real-time and spectroscopic SHG studies during the formation of thin layers of amorphous silicon (*a*-Si) by low energy Ar^+-ion bombardment by using a Ti:sapphire oscillator. In these studies, we observed a strong increase in SHG intensity upon ion bombardment and we showed that the SHG signal is originating from a dominant buried interface contribution near the *c*-Si E_0'/E_1 CP energy and an additional contribution from the *a*-Si surface.[46] Epitaxial growth of Si thin films has also been studied by SHG, however, only during dissociative chemisorption of Si_2H_6 on clean *c*-Si surfaces at high temperatures (>750 K). In these experiments, it was found that the SHG response was predominantly governed by variations in H coverage.[38,47] In this work, we focus on the interface formation between *c*-Si and Si thin films, both amorphous and epitaxial, during low temperature hot-wire chemical vapor deposition (HWCVD) by using a tunable Ti:sapphire laser for the SHG experiments.

III. EXPERIMENT

A. High vacuum reactor and deposition procedure

The Si thin films were deposited in a high vacuum reactor with a base pressure of $<10^{-9}$ mbar. The setup consists of two independently pumped chambers separated by a flange with the substrate mount, as schematically shown in Fig. 2. The substrate temperature can be accurately controlled by a feedback system consisting of a radiative heater at the rear side of the sample in combination with thermocouples and a proportional-integral-derivative controller. The films were deposited from SiH_4 gas with HWCVD. The hot-wire source consists of a coiled 0.45 mm diameter tungsten filament that is resistively heated by a 10 A dc to 2000 ± 200 °C. Prior to deposition, a mechanical shutter is placed in front of the substrate to avoid any deposition during the onset period of the hot-wire source. The deposition chamber is back filled with SiH_4 and once the pressure has stabilized, the hot wire is activated, typically after 30 s. Finally, when the hot wire stably operates, typically after 10 s, the shutter is removed and the deposition starts. During deposition, the pressure in the reactor is 8×10^{-3} mbar. The SiH_4 used has a purity of over 99.995% and is led through an additional purifier before being injected in the high vacuum reactor. For the conditions applied, the radical flux toward the substrate can be estimated to be at least 2 orders of magnitude larger than the flux of possible contaminants toward the substrate.

B. Substrate preparation

The substrates (50×20 mm^2) were either standard *n*-type Si(100) wafers (Czochralski grown, *P* doped, resistivity of 10–30 Ω cm, thickness of 500 ± 25 μm) or undoped trapezoidally shaped Si(100) substrates (Harrick Scientific,

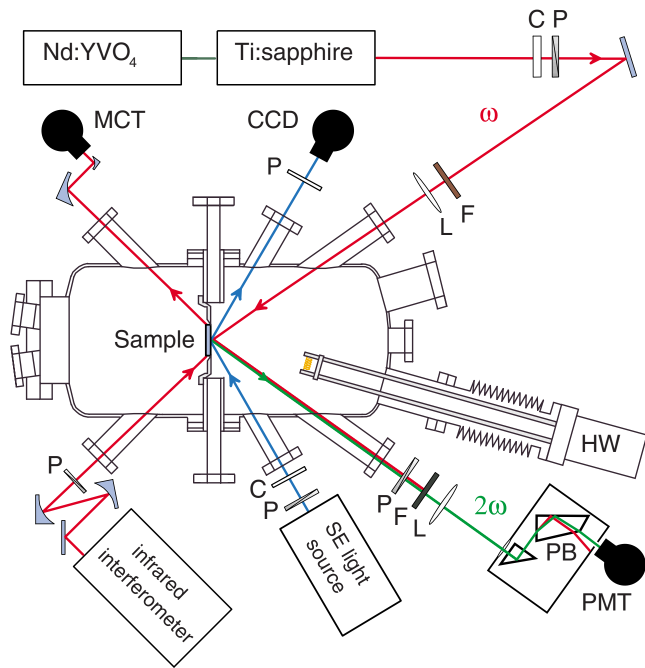

FIG. 2. (Color online) Schematic representation of the high vacuum setup used for the Si thin film depositions together with the three optical diagnostics: spectroscopic ellipsometry (SE), attenuated total reflection Fourier transform infrared spectroscopy (ATR-FTIR), and second-harmonic generation (SHG). The different components are indicated: wave plate (*C*), polarizer (*P*), optical filter (*F*), lens (*L*), Pellin Broca prism (PB), charge coupled device (CCD), HgCdTe detector (MCT), photomultiplier tube (PMT), and hot-wire source (HW).

thickness of 1 mm) with 45° angled bevels for experiments involving ATR-FTIR. Si thin films were deposited on both native oxide covered substrates and on H terminated substrates. The native oxide covered substrates were cleaned by immersion in an ultrasound ethanol bath for 20 min and blown dry with nitrogen. Two different sample cleaning procedures were applied to prepare the H terminated Si(100) substrates. Treatment A consisted of ultrasound cleaning in ethanol for 20 min, subsequent immersion in a 2% HF solution for 2 min, and finally rinsing with ultrapure water. Treatment B consisted of a standard RCA I and RCA II procedure by using a buffered 1% NH_4F/HF solution (BHF) with *p*H 4.[48] Both methods removed the native oxide terminating the *c*-Si surface with H. Directly after cleaning, the samples were mounted in the reactor oriented with the [011] crystal axis parallel to the plane of incidence of the optical techniques. Prior to deposition on the native oxide covered substrates and the HF cleaned substrates (treatment A), the setup was baked for 16 h with the samples reaching a temperature of 225 °C. The deposition on the RCA/BHF cleaned samples (treatment B) was started once reaching a substrate temperature of 150 °C and a background pressure of 10^{-7} mbar, typically <60 min after loading. The hot wire was placed at a distance of 11 cm from the native oxide and HF cleaned samples (A) and at a distance of 13 cm from the RCA/BHF cleaned samples (B). This resulted in deposition rates of 3.4 and 2.1 nm/min, respectively. The filament-substrate distance used and the deposition pressure of 8×10^{-3} mbar are close to the optimal conditions for hot-wire *a*-Si:H deposition as reported by Molenbroek *et al.*[49]

C. Optical setups

Optical access to the sample is provided by several viewports in the reactor. For the SE experiments, strain-free fused quartz windows (Bomco) were used. The SE experiments were performed at an angle of incidence of approximately 60° by using a rotating compensator spectroscopic ellipsometer (J.A. Woollam M-2000U) featuring a broadband light source (1.24–5.0 eV), polarization optics, and a charge coupled device (CCD) [see Fig. 2]. SE data were taken before, during, and after film deposition. By averaging 25 spectra, a good signal-to-noise ratio and a time resolution of 3.5 s were obtained for the real-time SE measurements. The SE data (Ψ,Δ) can be represented in a useful way in terms of the pseudodielectric function $\langle\varepsilon\rangle=\langle\varepsilon_1\rangle+i\langle\varepsilon_2\rangle$, which is calculated by treating the film and substrate as one semi-infinite material.[50] To facilitate the comparison with the SHG intensity, which is proportional to the squared second-order nonlinear susceptibility $|\chi^{(2)}|^2$, we will express the SE results mainly in terms of the squared pseudolinear susceptibility $|\langle\chi^{(1)}\rangle|^2$. The squared pseudolinear susceptibility is calculated from the pseudodielectric function by using $|\langle\chi^{(1)}\rangle|^2=(\langle\varepsilon_1\rangle-1)^2+\langle\varepsilon_2\rangle^2$. The SE data processing and analysis were performed by using the EASE 2.30 software package (J.A. Woollam).

The ATR-FTIR measurements were performed from the rear side of the substrates, as depicted in Fig. 2. The infrared radiation, entering and exiting the reactor through ZnSe windows, was provided by a Fourier transform infrared interferometer (Bruker Vector 22) and was focused on the bevels of the trapezoidally shaped substrates by parabolic gold mirrors. The interferometer operates in the frequency range of 400–7000 cm^{-1}; however, in this work, we focus on Si-H stretching vibrations in the 1800–2250 cm^{-1} range. A wire grid polarizer was used to polarize the incident radiation perpendicular to the plane of incidence (*s* polarization). The infrared beam underwent ~25 total internal reflections at each side of the sample (*c*-Si substrate and film), enhancing the sensitivity by a factor of ~50 compared to a single transmission measurement. After exiting the sample, the infrared beam was focused on a liquid nitrogen cooled HgCdTe (MCT) detector (Infrared Associates D313/6-M). During deposition, 15 scans were averaged, and with a spectral resolution of 4 cm^{-1}, this yielded a time resolution of 6.8 s. The ATR-FTIR data will be expressed in terms of absorbance A calculated from the measured transmission T and the background transmission T_0 obtained just before film deposition by using $A=-\log(T/T_0)$.

The fundamental laser radiation for the SHG experiments was provided by a Ti:sapphire oscillator (Spectra Physics Tsunami) that is tunable in the 1.35–1.75 eV photon energy range. This oscillator was pumped by an intracavity doubled cw $Nd:YVO_4$ laser (Spectra Physics Millennia Vsj). The repetition rate of the laser pulses was 80 MHz and the pulse duration was ~90 fs. Silver coated mirrors were used to

guide the laser beam into the reactor. With a variable wave plate and a Glan–Thompson polarizer, the polarization direction was selected and the laser power at the sample was set to 100 mW. Undesired radiation in the incident beam at the SHG radiation wavelength range was suppressed by a color filter (Schott OG570). The laser beam was focused onto the sample by using a plano convex BK7 lens. The radiation entered and exited the vacuum system through fused silica windows, which were verified not to generate any SHG radiation. The polarization direction of the SHG radiation was selected with a Glan–Laser polarizer. The fundamental radiation that reflected off the sample was suppressed both by spatial filtering applying a lens, a Pellin Broca dispersing prism, and a slit and by optical filters. For spectroscopic SHG experiments performed under steady-state conditions, two color filters were used (Schott BG40), while for the real-time SHG experiments performed during film deposition at a fixed fundamental photon energy (1.70 eV), a narrow band pass interference filter with a central wavelength of 365 nm and a full width at half maximum of 10 nm (Edmund Optics K43-103) was used. The latter filter was required to suppress not only the fundamental laser radiation but also stray light generated by the hot-wire source during deposition. In addition, an array of seven metal plates with concentric apertures and a mutual spacing of 10 mm was placed inside the vacuum chamber to suppress the stray light from the hot-wire source. The array was positioned in such a way that the diverging beam of fundamental and SHG radiation was tightly enclosed. It was verified that the combination of this array and the interference filter fully suppressed the stray light. The SHG radiation was detected by using a photomultiplier tube (Hamamatsu R585) connected to photon counting electronics. The beam waist of the laser beam at the sample was $\sim 100\ \mu$m. With an angle of incidence at the sample of 35°, this led to a fluence of $\sim 10\ \mu\mathrm{J/cm^2}$ per pulse. Under these conditions, no time-dependent variations in the SHG signal caused by photon-induced charge trapping were observed.[40] The time resolution for the real-time SHG experiments was 0.1 s and the dark count rate of the detection scheme was below 4 Hz. The SHG data will be represented in terms of the SHG intensity as calculated from the detected SHG signal after correction for the applied laser intensity and the response of the optical system. The optical response was obtained from separate transmission experiments of the optical components and was verified by spectroscopic SHG experiments on single side polished z-cut quartz. The second-order relation between the incident fundamental intensity and the SHG intensity was verified in the experiments. As mentioned in Sec. II, $\chi^{(2)}_{zzz}$, $\chi^{(2)}_{zxx}$, and $\chi^{(2)}_{xxz}$ are the only independent components of the second-order nonlinear susceptibility tensor that are nonzero for surfaces and interfaces of Si(100) and a-Si:H.[30,31] Depending on the selected polarization of the fundamental and SHG radiation, different tensor components contribute to the surface and interface SHG response, resulting in (local) maxima in the SHG signal for three different combinations: (1) p polarized fundamental and p polarized SHG radiation (pP polarization), where all three independent tensor components contribute, (2) s polarized fundamental and p polarized SHG radiation (sP polarization), where only $\chi^{(2)}_{zxx}$ contributes, and (3) mixed fundamental polarization with equal s and p components and s polarized SHG radiation (mix$S$ polarization), where only $\chi^{(2)}_{xxz}$ contributes. It should be noted that tensor component $\chi^{(2)}_{xxz}$ always occurs in combination with an inseparable isotropic bulk quadrupole susceptibility component γ of the substrate and/or film. The SHG experiments were mainly performed at pP polarization yielding the highest SHG intensity.

D. *Ex situ* diagnostics

In addition to the three optical techniques applied *in situ* during deposition, several *ex situ* diagnostics were used to characterize the Si thin films. As discussed above, carrier lifetime spectroscopy was used to measure the surface recombination velocity at the a-Si:H/c-Si interface for films deposited at different temperatures (Fig. 1). These photoconductance experiments were carried out by using a lifetime tester (Sinton Consulting WCT-100) in both quasisteady-state and transient mode.[14] The surface recombination velocity was calculated assuming an infinite bulk lifetime, which results in an upper limit for the surface recombination velocity. For these measurements, Si thin films with a thickness of 150–300 Å were deposited on both sides of 2 in. n-type Si(100) wafers (float zone, P doped, resistivity of 1.9 Ω cm, and thickness of 275 μm) by using sample treatment B. Information on the surface roughness was obtained by atomic force microscopy (AFM) using a vibration stabilized AFM (NT-MDT Solver P47) in noncontact mode with c-Si tips having a curvature radius of 10 nm. The absolute and spatially resolved hydrogen content in the films was measured with time-of-flight secondary ion mass spectrometry (TOF-SIMS). The analysis was carried out with an ION-TOF TOF-SIMS IV instrument at an operation pressure of $<1.5 \times 10^{-9}$ mbar. For sputtering 1 keV Cs^+ ions were used resulting in an erosion rate of about 7 Å/s, whereas either a Ga^+ or a Bi^+ gun was used as a primary ion source and secondary H^- ions were acquired. The film morphology was studied with cross sectional high resolution TEM. The samples were prepared by mechanical polishing by using the tripod method and were investigated using a FEI Tecnai F30ST microscope operated at 300 kV. The TOF-SIMS and the TEM analysis were carried out at Philips Research—Materials Analysis, Eindhoven, The Netherlands.

IV. RESULTS

A. Spectroscopic ellipsometry

In Fig. 3, the real and imaginary parts of the pseudodielectric function, $\langle\varepsilon_1\rangle$ and $\langle\varepsilon_2\rangle$, are shown as a function of photon energy for the native oxide covered and the H terminated Si(100) substrates at 150 °C just prior to deposition. The magnitude of the imaginary part of the dielectric function $\langle\varepsilon_2\rangle$ at the c-Si E_2 CP energy of 4.3 eV can be used to quantify the surface quality. The presence of any foreign material or microscopic roughness results in a decrease in the magnitude of the peak.[51] This feature was used to check the surface quality and to verify the result of the substrate treatment prior to every deposition on H terminated Si(100). In Fig. 3, the sensitivity to the nature of the surface is clearly

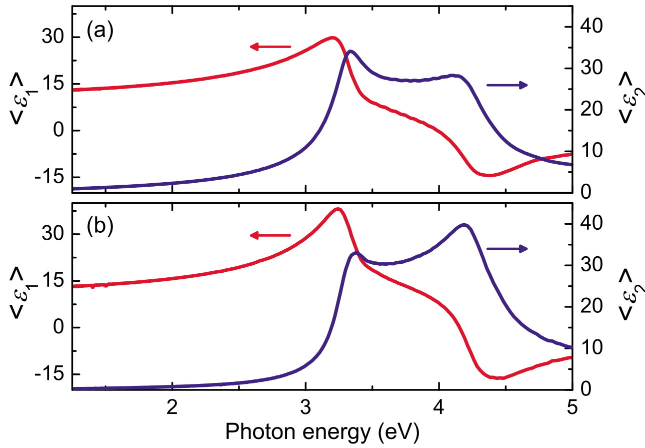

FIG. 3. (Color online) Real and imaginary parts of the pseudodielectric function as a function of photon energy at the deposition temperature of 150 °C for (a) native oxide covered Si(100) and (b) H terminated Si(100) substrates.

visible; obviously, the peak value for native oxide covered Si(100) is lower than for H terminated Si(100). However, also the two substrate treatments to obtain H terminated Si(100) resulted in slightly different peak values. Treatment A (B) resulted in $\langle\varepsilon_2\rangle=39.0\pm0.9$ (39.5 ± 0.9) at room temperature directly after cleaning and 38.1 ± 0.9 (38.6 ± 1.1) at 150 °C just prior to deposition. These values represent averages over the full sets of samples and, although the difference in $\langle\varepsilon_2\rangle$ after the two treatments is not significant, they might suggest a slightly higher quality surface after treatment B. The longer time between substrate cleaning and film deposition in treatment A due to the baking of the vacuum system did not cause a noticeable degradation of the surface quality. For both treatments, the values for $\langle\varepsilon_2\rangle$ suggest the presence of surface roughness, which is a known side effect of wet chemical etching of Si(100). With AFM, the surface roughness of the substrates was found to be below a rms value of 2 Å. For treatment B, the Si(100) surface roughness has been reported to be related to the presence of (111) facets.[52]

Figure 4 shows the squared pseudolinear susceptibility $|\langle\chi^{(1)}\rangle|^2$ as a function of photon energy measured with SE during Si film deposition at 150 °C. As a reference, also $|\langle\chi^{(1)}\rangle|^2$ of the native oxide covered and H terminated Si(100) substrates are shown as well as the linear susceptibility $|\langle\chi^{(1)}\rangle|^2$ of *a*-Si:H deduced from the SE data. The spectra in Figs. 4(a) and 4(b) were obtained during deposition on native oxide covered and H terminated Si(100) after treatment A, respectively, and show very similar trends. The films deposited on native oxide covered Si(100) exhibit a lower amplitude of $|\langle\chi^{(1)}\rangle|^2$ caused by the presence of the native oxide. With increasing film thickness, the difference between the two cases diminishes, as the impact of the substrate on the pseudolinear susceptibility decreases. The spectra in Figs. 4(a) and 4(b) clearly indicate the deposition of *a*-Si:H. With increasing film thickness, an evolution from a *c*-Si spectrum for the pristine substrate to an *a*-Si:H spectrum is visible; the *c*-Si E_0'/E_1 and E_2 CP resonances at 3.3 and 4.3 eV broaden and ultimately cannot be separately distinguished anymore.

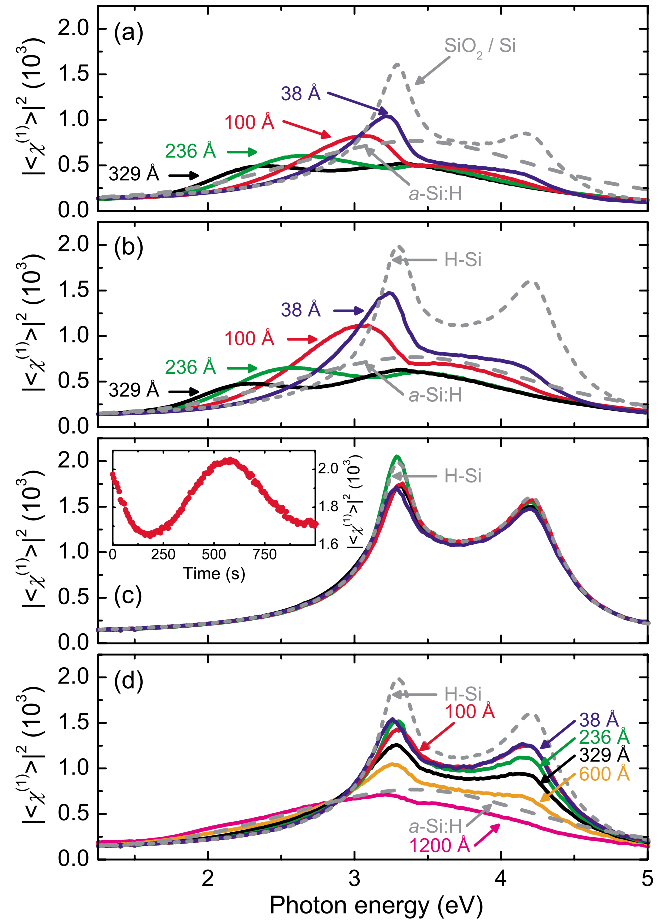

FIG. 4. (Color online) Squared pseudolinear susceptibility $|\langle\chi^{(1)}\rangle|^2$ obtained with SE during deposition at 150 °C for (a) *a*-Si:H on native oxide covered Si(100) and (b) *a*-Si:H, (c) epi-Si, and (d) mixed phase Si on H terminated Si(100). In (a)–(d), data are given for selected film thicknesses of 38, 100, 236, and 329 Å, with additional curves for 600 and 1200 Å films in (d). Dashed lines indicate $|\langle\chi^{(1)}\rangle|^2$ for the native oxide covered and H terminated Si(100) substrates and $|\chi^{(1)}|^2$ of *a*-Si:H as deduced from the data. The inset in (c) displays $|\langle\chi^{(1)}\rangle|^2$ at 3.3 eV as a function of deposition time for epi-Si films.

The spectra in Fig. 4(c) were obtained during deposition on H terminated Si(100) after treatment B and correspond to films with the same thickness as in Figs. 4(a) and 4(b). These spectra hardly change with increasing film thickness and coincide with the spectrum for the pristine H terminated Si(100) substrate, which reveals that the films developed epitaxially. In Fig. 4(d), also obtained during deposition on H terminated Si(100) after treatment B, an intermediate situation is visible. The spectra change with increasing film thickness; however, the characteristic crystalline features remain present. This slow evolution from a *c*-Si spectrum to an *a*-Si:H spectrum indicates the deposition of mixed phase material consisting of both amorphous and epitaxial Si.

Van den Oever *et al.* described the evolution of the dielectric function, bulk thickness, and surface roughness of *a*-Si:H deposited on native oxide covered Si(100) as obtained from optical model-based analysis of real-time SE data.[24] The thicknesses of the different *a*-Si:H films, as in-

dicated in Fig. 4, have been obtained by using a similar approach. However, for the films deposited on H terminated Si(100), the analysis yields significantly higher residue values between data and model during initial film growth (<20 Å) than for films deposited on native oxide covered substrates. These higher residues are caused by a lack in optical contrast between the Si films and the H terminated Si(100) substrates. A consequence of this lack in contrast is that initial changes in SE data cannot clearly be assigned to the presence of a certain film morphology, surface roughness, or contamination for these ultrathin films.

The similarity between all spectra in Fig. 4(c) does not only indicate the deposition of epi-Si films, it also suggests that the surface roughness does not significantly change with film thickness. Apparently, the surface roughness remains of a comparable magnitude as the surface roughness of the substrate. As discussed above, an increase in surface roughness would yield a monotonously decreasing trend in $\langle\varepsilon_2\rangle$ and hence also in $|\langle\chi^{(1)}\rangle|^2$, especially at the E_2 CP energy. This decreasing trend is not observed. $|\langle\chi^{(1)}\rangle|^2$ displays, however, an oscillation as a function of film thickness. The inset in Fig. 4(c) shows this oscillation as a function of deposition time at a photon energy of 3.3 eV. Teplin *et al.* attributed this behavior to interference due to the presence of a porous interface layer possibly related to a higher hydrogen content at the interface.[7] For the a-Si:H films in Figs. 4(a) and 4(b), interference fringes in the 2–3 eV photon energy range are visible. The presence of these fringes indicates that the interface between the native oxide covered and H terminated c-Si substrates and the deposited films is relatively sharp. In the spectra in Fig. 4(d) obtained during deposition of mixed phase material, these interference fringes are absent, indicating that the contrast between the c-Si substrate and the film is limited. This suggests that the mixed phase film developed as a graded layer, with an increasing a-Si:H content with increasing thickness.

The a-Si:H content in the mixed phase material in Fig. 4(d) has been deduced by using two different three-layer optical models to describe epitaxial breakdown, which are similar to the models used by Teplin *et al.*[7] The first model consists of (1) a c-Si substrate, (2) a graded layer modeled as an effective medium of crystalline and amorphous material, and (3) a surface roughness layer. The optical constants for the c-Si substrate are extracted from the SE data obtained prior to deposition in terms of the pseudodielectric function, as shown in Fig. 3(b). The same optical constants are used for the crystalline fraction in the graded layer. The optical constants for the amorphous fraction in the graded layer were described with the Cody–Lorentz formalism with parameters determined from the topmost, fully amorphous material formed at the end of the deposition.[24,53] The dielectric function of the film was assumed to linearly vary from pure c-Si to pure a-Si:H over the thickness of the film. The surface roughness layer was modeled as an effective medium consisting of 50% voids and 50% of the underlying material by using the Bruggeman approximation.[54] The thickness of the graded film and the thickness of the surface roughness layer were included in the fitting process. In the second model, a virtual interface approach was applied.[55] The optical model consists of (1) a virtual substrate, (2) a thin effective medium layer of crystalline and amorphous material, and (3) a surface roughness layer that was treated the same way as in the graded layer model. In this approach, the real-time SE data measured in a certain time interval are fitted by assuming that SE data measured before this interval can be converted into optical constants of an effective substrate. The amorphous content of the overlying effective medium layer, having a thickness of typically 25 Å, is fitted by using the same Cody–Lorentz parameters for the a-Si:H as in the linear grade model. The surface roughness is also fitted in this virtual interface approach. The a-Si:H content resulting from the real-time SE analysis using both the linear grade and virtual interface models is shown in Fig. 5. Both models yield similar results and show a linear increase in the a-Si:H content with thickness. It can be concluded that the initial film growth was predominantly epitaxial, whereas the film growth at the end of the deposition (i.e., at a film thickness of ~1200 Å) was fully amorphous. The thickness of the surface roughness layer at the end of the deposition was around 20 Å in both models. In summary, with spectroscopic ellipsometry, the optical properties of the Si thin films have been characterized in terms of the pseudolinear susceptibility. Also, information on the film thickness and surface roughness has been obtained. From the SE data, different film morphologies can be distinguished in real time during processing, and in addition, the technique provides information on the abruptness of the film/substrate interface.

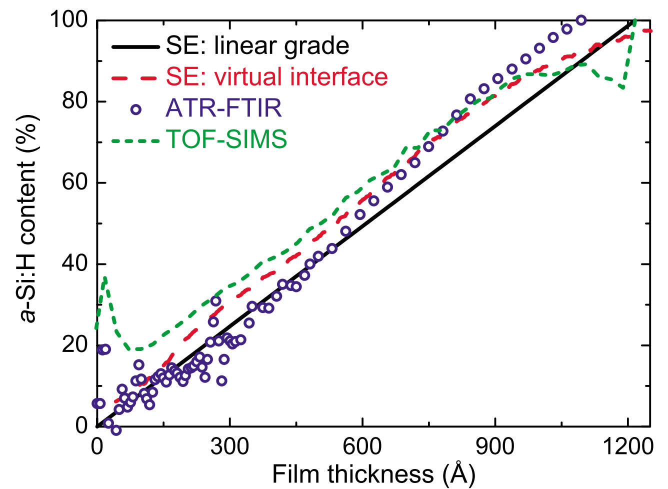

FIG. 5. (Color online) Fraction of a-Si:H in a mixed phase Si film on H terminated Si(100) as a function of film thickness as deduced from SE using linear grade analysis and virtual interface analysis, and as deduced from the H content in the film obtained by ATR-FTIR and TOF-SIMS.

The surface roughness of the different films has also been investigated with AFM. Figure 6 shows the AFM micrographs for a-Si:H deposited on native oxide covered Si(100) and a-Si:H, epi-Si, and mixed phase Si on H terminated Si(100). The rms roughness of the different films deduced from the AFM data is also indicated in Fig. 6. The results correspond well to the results obtained with SE. It is clear that epi-Si films exhibit the lowest surface roughness. The rms roughness of these films is ~3 Å and is therefore comparable to the roughness of the substrates (<2 Å). The sur-

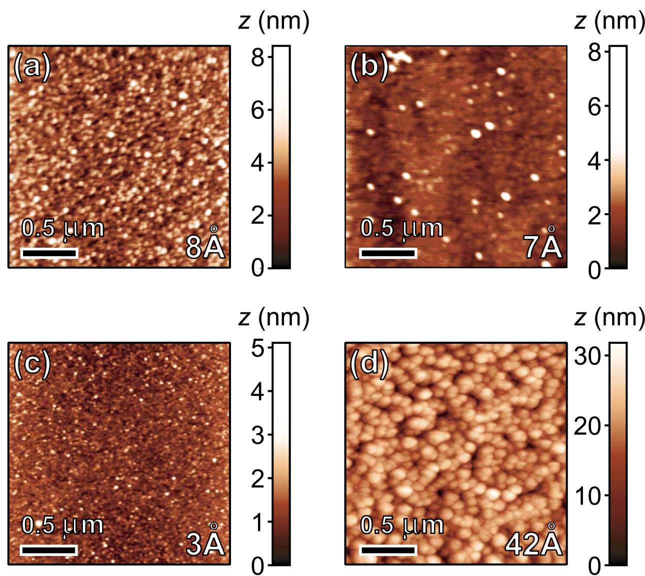

FIG. 6. (Color online) AFM micrographs for (a) 3500 Å of *a*-Si:H on native oxide covered Si(100), (b) 329 Å *a*-Si:H on H terminated Si(100), (c) 350 Å epi-Si on H terminated Si(100), and (d) a 3140 Å thick film that consists of mixed phase Si, with the first ~250 Å being epi-Si. The rms roughness of the films is indicated in the figure.

face roughness of the *a*-Si:H films is somewhat larger, but still below a rms value of 10 Å. The mixed phase material yields the highest surface roughness, possibly related to a slightly different growth rate between the amorphous and epitaxial phase in the film, as also found by Teplin *et al.*[56]

B. Attenuated total reflection infrared spectroscopy

Figure 7 shows the absorbance as a function of frequency measured with ATR-FTIR during the deposition of Si thin films. The spectra in Fig. 7(a) were obtained during deposition of *a*-Si:H on native oxide covered Si(100), the spectra in Fig. 7(b) during deposition of *a*-Si:H on H terminated Si(100) after treatment A, and the spectra in Fig. 7(c) during deposition of mixed phase Si on H terminated Si(100) after treatment B. The absorbance in the 1900–2200 cm^{-1} range can be assigned to SiH_x stretching modes of hydrogen in the bulk and at the surface of the films.[21,22,25,27,28,57,58] It can be seen that for similar thickness values, the absorbance for the *a*-Si:H films is about an order of magnitude higher than for the mixed phase material, indicating a higher H content in the amorphous material. With increasing film thickness, the absorbance increases for all films, whereas the position of the peak absorbance value shifts toward lower frequencies for thicker films.

To obtain quantitative information about the hydrogen bonding in the films as a function of film thickness, the spectra were deconvoluted into several Gaussian peaks. The peak assignments are based on reports in literature and are summarized in Table I. Figure 7(d) shows the deconvolution of the spectrum for 38 Å *a*-Si:H on H terminated Si(100) [cf. Fig. 7(b)], which can be reproduced very well by three relatively narrow peaks due to SiH_x surface modes and two

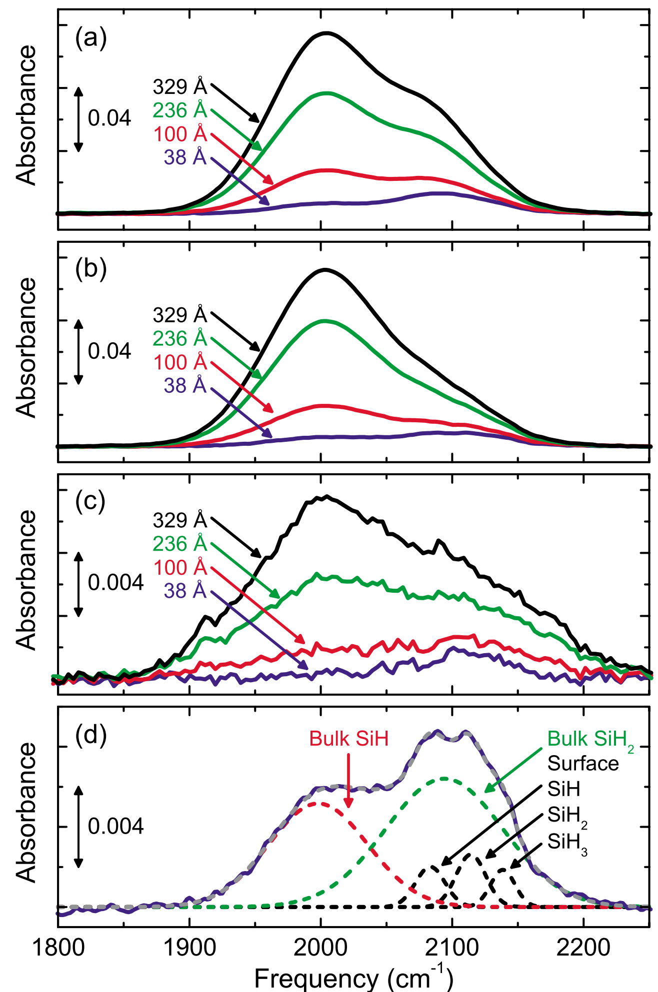

FIG. 7. (Color online) ATR-FTIR spectra for (a) *a*-Si:H on native oxide covered Si(100), (b) *a*-Si:H on H terminated Si(100), and (c) mixed phase Si on H terminated Si(100). For clarity, only data for selected film thicknesses of 38, 100, 236, and 329 Å are shown. In (d), the deconvolution of the spectrum for 38 Å *a*-Si:H on H terminated Si(100) is shown, including the assignment of the peaks.

broader peaks related to SiH and SiH_2 bulk modes.[21,22,25,27,28] For the *a*-Si:H films deposited on native oxide covered Si(100), oxygen back bonded SiH_x modes

TABLE I. The range of center peak positions of the infrared absorption peaks in the SiH_x stretching region of *a*-Si:H and their assignments (Refs. 21, 22, 25, 27, 28, and 57). The full width at half maximum of bulk peaks and surface peaks are ~85 and ~25 cm^{-1}, respectively.

Peak position (cm^{-1})	Assignment
1980–2020	Bulk SiH
2070–2105	Surface SiH
2080–2095	Bulk SiH_2
2110–2120	Surface SiH_2
2135–2145	Surface SiH_3
2155–2165	Surface SiH_2 on SiO

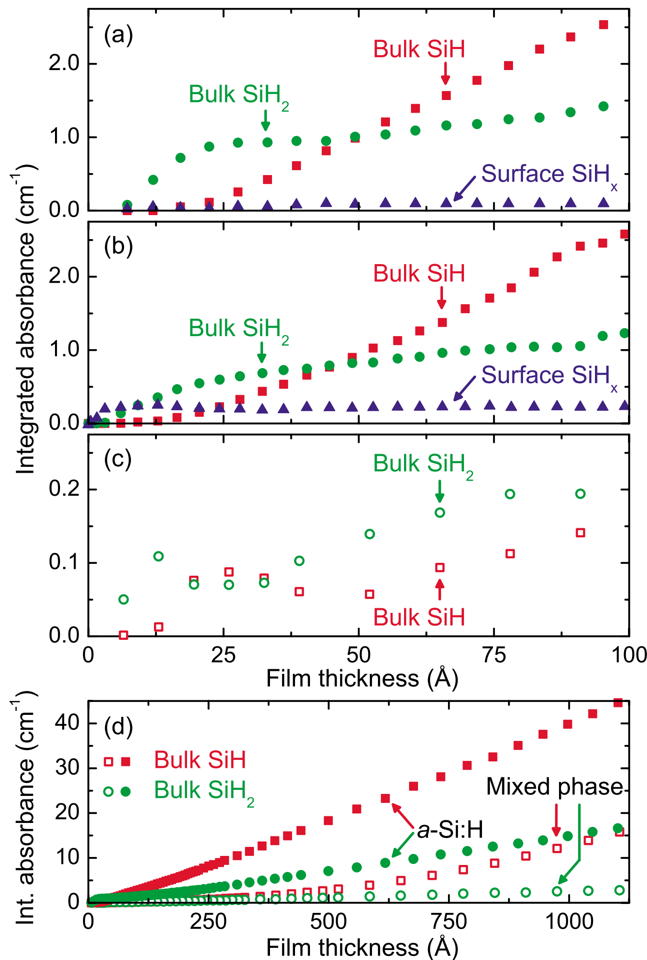

FIG. 8. (Color online) Integrated absorbance by SiH and SiH_2 bulk stretching modes and the total SiH_x surface stretching modes as a function of film thickness for (a) *a*-Si:H on native oxide covered Si(100), (b) *a*-Si:H on H terminated Si(100), and (c) mixed phase Si on H terminated Si(100). In (d), the integrated absorbance by SiH and SiH_2 bulk modes for *a*-Si:H on native oxide covered Si(100) and mixed phase Si on H terminated Si(100) are shown in one plot up to a film thickness >1000 Å.

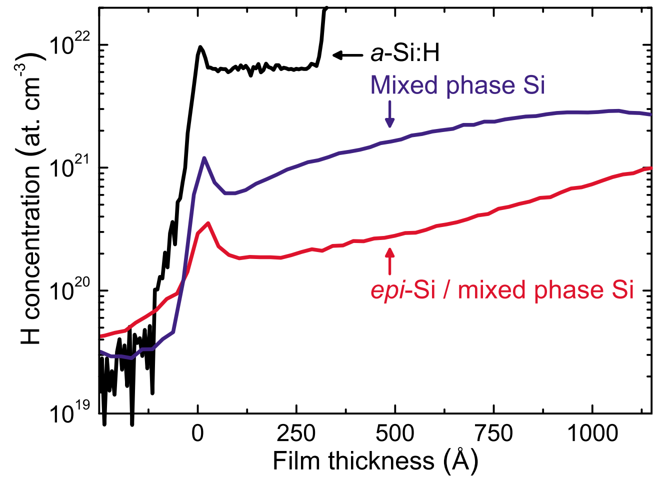

FIG. 9. (Color online) H content in *a*-Si:H, mixed phase Si, and epi-Si as obtained with TOF-SIMS. The epi-Si film displayed breakdown into mixed phase Si at a thickness of ~250 Å. The positive (negative) horizontal axis denotes the film (substrate) region.

were also detected.[57] Due to the limited absorbance, surface peaks could not be distinguished from bulk modes in mixed phase material. In Figs. 8(a)–8(c), the integrated absorbance by SiH and SiH_2 bulk modes and the sum of the integrated absorbance by SiH_x surface modes resulting from the deconvolution of the ATR-FTIR spectra are shown at the onset of film growth as a function of film thickness. Data are presented for *a*-Si:H on native oxide covered Si(100), *a*-Si:H on H terminated Si(100), and mixed phase Si on H terminated Si(100), respectively. As is visible from Fig. 8(b), the absorbance by SiH_x surface modes is dominant at the onset of *a*-Si:H deposition on H terminated Si(100). Subsequently, the absorbance by the SiH_2 bulk mode strongly increases. For *a*-Si:H deposited on native oxide covered Si(100), shown in Fig. 8(a), the initial increase in the absorbance by the SiH_2 bulk mode is even stronger. These phenomena indicate a H-rich onset of *a*-Si:H film growth. Although a high H density might cause a poor initial network structure,[22,25] this H-rich interface region can be beneficial for the surface passivation properties of the *a*-Si:H films on H terminated Si(100). After ~40 Å of *a*-Si:H deposition on H terminated Si(100), the SiH bulk mode becomes dominant. The integrated absorbance for the mixed phase Si, shown in Fig. 8(c), is very low for ultrathin films, which indicates that initially the H content and hence the *a*-Si:H fraction are very low.

In Fig. 8(d), the integrated absorbance by SiH and SiH_2 bulk modes is displayed for thicker films. The integrated absorbance of *a*-Si:H deposited on H terminated Si(100) is omitted in Fig. 8(d), as the data are very similar to the integrated absorbance of native oxide covered Si(100) substrates, especially at this scale. The integrated absorbance by SiH and SiH_2 bulk modes for *a*-Si:H linearly increases as a function of film thickness, indicating a constant H content during bulk film growth. This H content can be calculated to be around 12.5 at. %. However, for the mixed phase material, the absorbance by SiH and SiH_2 bulk modes increases with thickness, which indicates an increase in the *a*-Si:H fraction. By assuming that all H in the film can be attributed to *a*-Si:H, the *a*-Si:H fraction in the mixed phase material can be calculated from the H content. The resulting *a*-Si:H fraction as a function of film thickness is shown in Fig. 5, in which also the *a*-Si:H fraction in the mixed phase material as obtained by SE was displayed. It can be seen that the *a*-Si:H fraction calculated from the ATR-FTIR data corresponds very well to the results obtained with SE. The ATR-FTIR data also show that the initial film growth was predominantly epitaxial, whereas the *a*-Si:H fraction increased almost linearly with film thickness. Concluding, the characterization of the H bonding in the Si thin films by ATR-FTIR allows for real-time distinction between different Si film morphologies.

The H content in the *a*-Si:H and mixed phase material was also measured by TOF-SIMS, as shown in Fig. 9. In Fig. 9 also the H content is displayed for a film that developed fully epitaxial for the first ~250 Å and subsequently broke down into mixed phase material. These data correspond very

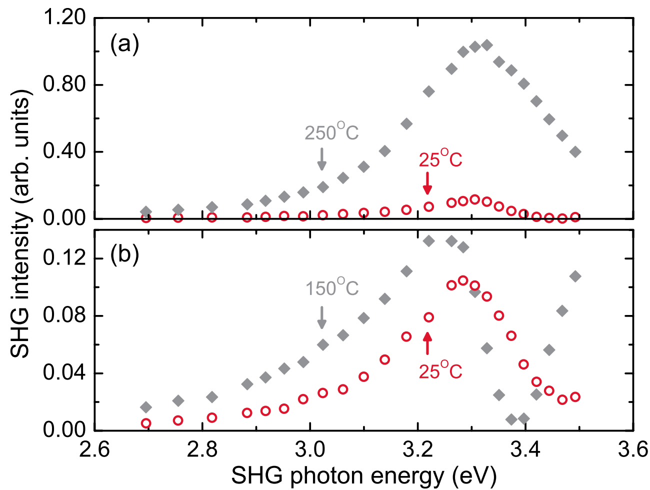

FIG. 10. (Color online) SHG spectra for *pP* polarization for (a) native oxide covered Si(100) and (b) H terminated Si(100) substrates both at room temperature and at the deposition temperature.

well to the results obtained with ATR-FTIR. As is visible from Fig. 9, for all films, the interface between substrate and film is relatively H rich. For the *a*-Si:H, the H content is constant throughout the film, which is around 6×10^{21} cm^{-3} or 12 at. %. The strong increase in H content at ~300 Å is due to H present at the surface. The H content in the mixed phase film is initially about an order of magnitude lower than for *a*-Si:H and increases with film thickness. For the film with initial epitaxial growth, the H content is even lower. During bulk epi-Si growth, the H content is constant, whereas the breakdown into mixed phase material is clearly visible from the increase in H content after reaching a thickness of ~250 Å. Similar as for the ATR-FTIR analysis, the *a*-Si:H fraction in the mixed phase film has been calculated from the H content in Fig. 9 by assuming that all H can be attributed to *a*-Si:H. This result is also displayed in Fig. 5 and corresponds very well to the results obtained with SE and ATR-FTIR.

C. Spectroscopic second-harmonic generation

Both SE and ATR-FTIR are useful diagnostics to measure Si thin film properties in real time during processing. However, as these techniques predominantly probe bulk properties, their sensitivity is inherently limited during the initial film growth (<20 Å). For SE, this is caused by the limited contrast between the Si film and Si substrate. The limited sensitivity of ATR-FTIR arises from the very low absorbance values at the onset of film growth. As for many applications of *a*-Si:H and epi-Si films on *c*-Si, the interface properties are essential for a good device performance; information on the initial film growth is highly desired. Because of its sensitivity to surfaces and interfaces, the nonlinear optical technique of second-harmonic generation has the potential to provide this information at the onset of growth of Si films.

In Fig. 10, the SHG spectra for native oxide covered and H terminated Si(100) substrates are shown. The results are clearly different for the two situations and illustrate the sensitivity of SHG to the nature of the substrate surface. For both situations, a strong dependence on substrate temperature is observed. The SHG spectrum for native oxide covered *c*-Si at room temperature is clearly asymmetric and consists of several interfering contributions. Furthermore, this spectrum corresponds well to the spectra reported by Rumpel *et al.* for SiO_2/Si(100), which were shown to consist of (1) a contribution related to Si-Si bonds modified due to the presence of the SiO_2/*c*-Si interface with a resonance at 3.3 eV near the *c*-Si E_0'/E_1 CP energy, (2) an EFISH contribution related to the *c*-Si bulk SCR at the E_0'/E_1 CP energy of 3.4 eV, and (3) nonresonant contributions near 3.7 eV related to Si atoms bonded to SiO_2 and near 4.3 eV at the *c*-Si E_2 CP energy, respectively.[42] At the deposition temperature of 250 °C, the SHG spectrum has a more symmetric appearance and the amplitude has increased with almost an order of magnitude. This effect is caused by a strong increase in the EFISH contribution, reflecting the temperature dependence of the bulk Fermi level.[38] The EFISH contribution dominates the SHG spectrum at this elevated temperature. The increased temperature has also redshifted and broadened the *c*-Si E_0'/E_1 CP resonance, which is an effect that is well known from linear optical techniques such as SE. The SHG spectra for H terminated Si(100) correspond well to SHG spectra reported by Dadap *et al.* for H terminated Si(100) prepared by exposing Si(100) to atomic H after removing the native oxide by a controlled heat flash.[38] The spectra show a maximum at 3.25 eV and a sharp minimum at 3.4 eV at 150 °C that blueshift with decreasing temperature. This similarity with the results by Dadap *et al.* corroborates that the wet chemical cleaning applied in the present study provided a good H termination of the *c*-Si surface. As reported by Dadap *et al.*, the spectra for H terminated Si(100) can be explained by (1) a contribution related to interface-modified Si-Si bonds near 3.3 eV, (2) a surface EFISH contribution near 3.4 eV, and (3) a nonresonant contribution at higher photon energy.[38] Interference of these contributions results in the sharp minimum at 3.4 eV in the 150 °C spectrum. The different temperature dependence of the interfering contributions causes the difference between the spectra at RT and at 150 °C. The absence of the strong increase in amplitude with increasing temperature indicates that bulk EFISH does not play a important role for the H terminated Si(100), in contrast to the case for the native oxide covered Si(100).[38]

In Fig. 11, SHG spectra for *a*-Si:H thin films deposited on native oxide covered Si(100) as measured at the deposition temperature of 250 °C are shown. These spectra have a similar symmetric appearance as the spectrum for the pristine substrate. The spectral feature for 97 Å *a*-Si:H has nearly the same amplitude and width as the feature obtained for the substrate itself and shows a slight blueshift. The spectra for 249 and 300 Å thick films show redshifted and broader features with lower amplitudes, which is an effect that is stronger for the thicker film. In the inset of Fig. 11, the SHG spectrum for 97 Å *a*-Si:H at 250 °C is shown together with the spectrum for the same film at room temperature. With decreasing temperature, the spectral feature blueshifts to 3.4 eV, narrows, and increases in amplitude. These trends were also observed for the other films (not shown). From the similarity between the spectra for the thin films and the spec-

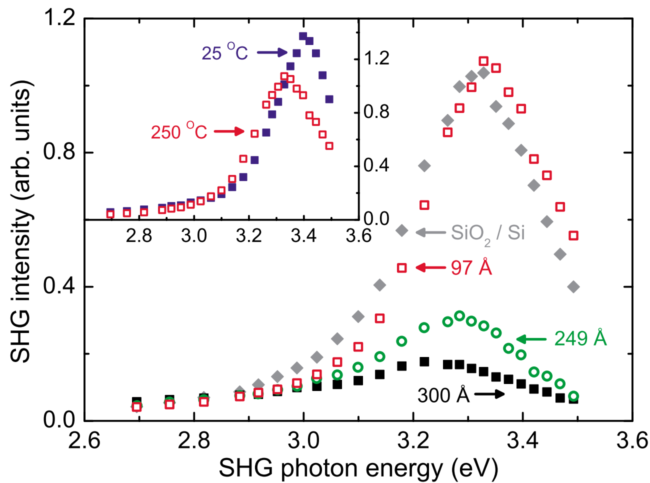

FIG. 11. (Color online) SHG spectra for *pP* polarization for *a*-Si:H films with a thickness of 97, 249, and 300 Å deposited on native oxide covered Si(100) at 250 °C. The spectrum for the native oxide covered substrate itself is also shown. The inset shows the comparison between the SHG spectra for the 97 Å thick *a*-Si:H film as measured at 250 °C and at room temperature.

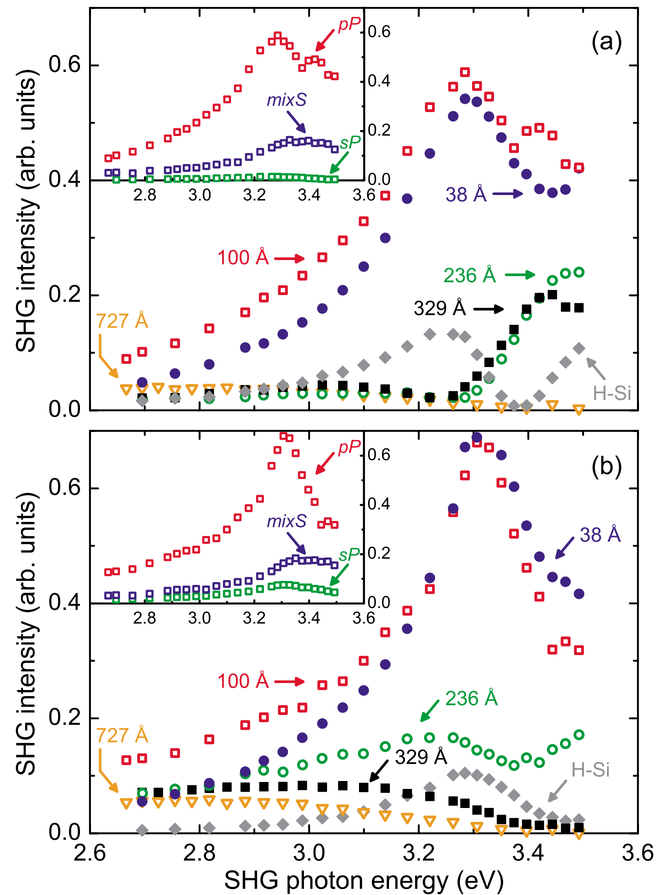

FIG. 12. (Color online) SHG spectra for *pP* polarization for *a*-Si:H with a thickness of 38, 100, 236, 329, and 727 Å deposited on H terminated Si(100), together with the spectra for the pristine H terminated Si(100) substrate, as measured at (a) the deposition temperature of 150 °C and (b) room temperature.

trum for the substrate, it can be concluded that also the SHG signal for the *a*-Si:H films is dominated by EFISH at the E_0'/E_1 CP energy arising from the *c*-Si SCR. The behavior for thicker films can be explained by absorption of SHG radiation that is generated at the interface region with the *c*-Si and that propagates through the *a*-Si:H films.[46] The SHG radiation is strongly absorbed when propagating through the *a*-Si:H, especially at higher photon energies. This causes not only a decrease in amplitude but also broadening and an effective redshift of the spectral feature. The low SHG intensity for thicker films is consistent with the weak SHG response reported by Erley and Daum for a 0.7 μm thick *a*-Si:D film on Si(100).[41] The slight blueshift of the spectral feature of the 97 Å film compared to the response of the pristine substrate might be related to an additional contribution from the buried interface between *a*-Si:H and SiO_2 or from the *a*-Si:H surface. However, the strong decrease in SHG signal for thicker films indicates that the *a*-Si:H surface can be expected to have a minor influence. The blueshift and narrowing of the spectral feature with decreasing temperature corresponds to the temperature behavior of the E_0'/E_1 CP resonance, as known from linear optics and also observed for the native oxide covered substrates. The maximum at a SHG photon energy of 3.4 eV in the SHG spectrum obtained at room temperature corroborates the dominance of the EFISH contribution.[38] However, the strong temperature dependence of the amplitude of the SHG intensity observed for the native oxide covered substrates is absent.

SHG spectra for *a*-Si:H thin films deposited on H terminated Si(100) obtained at the deposition temperature of 150 °C are shown in Fig. 12(a). These spectra clearly differ from the spectra for *a*-Si:H deposited on native oxide covered Si. For ultrathin *a*-Si:H films of 38 and 100 Å, the SHG intensity is enhanced compared to the pristine H terminated Si(100) substrate. Furthermore, the SHG intensity for these *a*-Si:H films has a sharp maximum at 3.3 eV and an additional feature above 3.4 eV. The spectra have a lower amplitude and are broader and less symmetric than the spectra for *a*-Si:H films with comparable thickness deposited on native oxide covered Si(100). For the 236 and 329 Å films, the intensity is reduced again, showing a minimum around 3.25 eV and a maximum around 3.5 eV. For a thick film of 727 Å, the SHG intensity is very low, particularly in the high photon energy range. In Fig. 12(b), SHG spectra at room temperature for the same films are depicted. These spectra show similar trends as the spectra at the deposition temperature: sharp maxima near 3.3 eV for the ultrathin films of 38 and 100 Å and a decreasing SHG intensity with increasing film thickness. However, for the ultrathin films, the peaks in the spectra obtained at room temperature have a reduced width, an increased amplitude, and a slightly blueshifted photon energy, which result in a more symmetric appearance compared to the spectra measured at 150 °C. Furthermore, the minimum for the 236 Å film has become less pronounced, whereas it is not visible anymore for the 329 Å film.

The decreasing SHG intensity for thicker *a*-Si:H films can be explained by SHG radiation that is absorbed while propagating through the film, which is similar as discussed

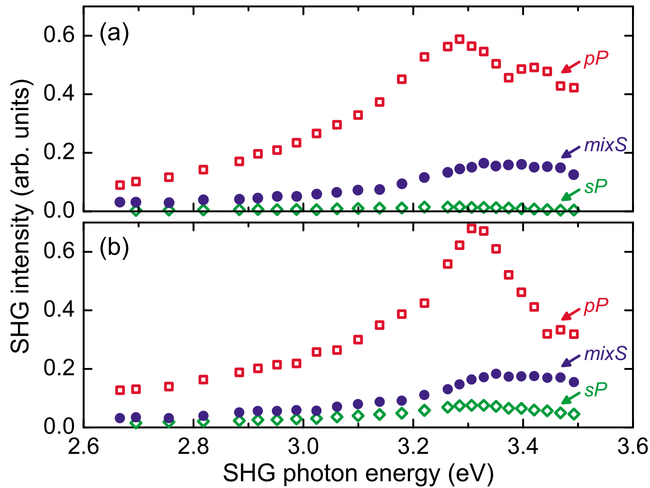

FIG. 13. (Color online) SHG spectra for *pP*, mix*S*, and *sP* polarization for *a*-Si:H with a thickness of 100 Å deposited on H terminated Si(100) at (a) the deposition temperature of 150 °C and (b) room temperature.

above for *a*-Si:H deposited on native oxide covered Si(100). This observation suggests that also for *a*-Si:H deposited on H terminated Si(100), the SHG radiation is predominantly generated at the buried interface with *c*-Si. To verify this hypothesis, the SHG response was recorded during exposure of a 105 Å thick *a*-Si:H film to molecular oxygen directly after deposition. The oxygen (purity 99.999%) was injected through a leak valve into the reactor for 225 s, resulting in total dose of 1.7×10^5 L. The SHG intensity, which is measured at a SHG photon energy of 3.40 eV, increased by only ~6%, whereas the SHG spectrum remained very similar to the spectrum of the 100 Å film shown in Fig. 12(a). As the oxygen is expected to only influence the film surface, this limited response is in line with the conclusion that the SHG signal is predominantly originating from the buried interface. The result of the oxygen dosing is consistent with the observations reported by Aarts *et al.* for *a*-Si:H films deposited on fused silica.[45]

In Figs. 13(a) and 13(b), the *pP* polarized spectra for the 100 Å film are shown together with the spectra for mix*S* and *sP* polarization at the deposition temperature and room temperature, respectively. At both temperatures, the SHG intensity obtained at these two polarization combinations is lower than for *pP* polarization. The spectra for mix*S* polarization show a maximum around 3.4 eV, while the *sP* spectra have a peak near 3.3 eV. As addressed in Sec. III C, the components of the second-order nonlinear susceptibility tensor that contribute to the SHG response depend on the polarization combination selected. For *sP* polarization, tensor component $\chi^{(2)}_{zxx}$ contributes, which is inseparable from the isotropic bulk quadrupole susceptibility component γ. The low SHG response observed for *sP* polarization directly implicates that isotropic bulk contributions from both the film and the substrate have limited influence and can only play a marginal role in the spectra for *pP* polarization. Moreover, the strong intensity increase observed in the *pP* polarized spectra for thin *a*-Si:H films compared to the spectrum for the H terminated substrate suggests that the influence of bulk contributions from the substrate (i.e., isotropic as well as anisotropic contributions) is limited. The SHG intensity for mix*S* polarization, where only tensor component $\chi^{(2)}_{xxz}$ contributes, is also significantly lower than for *pP* polarization; this suggests that tensor component $\chi^{(2)}_{zzz}$ is dominant in the response for *pP* polarization. The thickness dependence of the spectra for mix*S* and *sP* polarization (not shown) is similar as for *pP* polarization; the SHG intensity increases with thickness for films with a thickness below 10 nm, while beyond this thickness, the intensity decreases again, particularly at high photon energies. These trends indicate that the SHG response for mix*S* and *sP* polarization is also dominated by the buried interface, similar as for *pP* polarized spectra.

The somewhat broader and less symmetric appearance of the *pP* polarized SHG spectra for *a*-Si:H films deposited on H terminated Si(100) compared to the spectra for *a*-Si:H films on native oxide covered Si(100) indicates that the spectra for the *a*-Si:H films on H terminated Si(100) consist of multiple contributions. A deconvolution of these spectra into separate resonances might provide more insight into the exact microscopic origin of the SHG response after *a*-Si:H deposition and the changes with respect to the H terminated substrates.[46,59] This method has been successfully applied for SHG experiments on amorphous Si layers formed by ion bombardment of H terminated Si(100).[46] However, for the present case, the SHG spectra for different film thicknesses could not yet be consistently reproduced. Therefore, the spectra are qualitatively analyzed, which also yields important information on the origin of the SHG response.

For example, the SHG spectra for ultrathin *a*-Si:H films of 38 and 100 Å on H terminated Si(100) have a similar shape as the linear susceptibility for *c*-Si with a sharp resonance at 3.3 eV (cf. Fig. 4). This indicates that also these SHG spectra include a dominant contribution related to the *c*-Si E_0'/E_1 CP transition. Also the trends observed in the spectra for these films with decreasing temperature, i.e., the narrowing and the slight blueshift of the maxima, are characteristic for the E_0'/E_1 CP transition and are also observed for *a*-Si:H films on native oxide covered substrates. This contribution is interfering with an additional smaller and broader contribution originating probably from Si-Si bonds of *a*-Si:H.[45,46] Also, nonresonant contributions, e.g., at the *c*-Si E_2 CP energy, might influence the SHG spectra. Similar as discussed above for the H terminated substrates, the different temperature dependences of the interfering contributions account for the differences between the spectra obtained at 150 °C and at room temperature.

In general, SHG contributions near the *c*-Si E_0'/E_1 CP energy might be related both to Si-Si bonds in the *c*-Si modified due to the presence of the interface with the *a*-Si:H and to EFISH effects. However, in contrast to the spectra for the *a*-Si:H films on native oxide covered substrates, a dominant contribution of EFISH to the SHG spectra in Fig. 12 is unlikely. At room temperature, EFISH would result in a clear resonance at 3.4 eV (cf. Fig. 11),[38] whereas the room temperature *pP* polarized spectra for both 38 and 100 Å thick *a*-Si:H on H terminated Si(100) display a sharp peak at the lower SHG photon energy of 3.3 eV. The redshift of the resonance to 3.3 eV with respect to the room temperature E_0'/E_1 CP energy of bulk *c*-Si of 3.4 eV indicates that modi-

fied or weakened Si-Si bonds in the *c*-Si in the interface region with the *a*-Si:H film are more likely responsible for the SHG response.[37,41] In principle, interference of multiple SHG contributions can also effectively shift a resonance. However, it is unlikely that this effect has caused the large shift from 3.4 to 3.3 eV, as this effect would also result in a highly asymmetric spectrum. This is not in agreement with the sharp and symmetric spectra observed for the 38 and 100 Å thick *a*-Si:H films at room temperature. The increase in amplitude of the spectra for the *a*-Si:H covered Si(100) and the spectra for the pristine H terminated Si(100) suggests that the nature of the Si(100) surface has changed after *a*-Si:H deposition. Also, the presence of a thin film can, in principle, enhance the efficiency of SHG from an underlying substrate interface compared to a bare substrate surface. This enhancement can arise because of multiple reflections of both the fundamental and the SHG radiation within the film resulting in interference effects. However, by calculating the linear propagation effects of the fundamental and the SHG radiation in the film,[46] it can be shown that the film should be fully transparent to both the fundamental and the SHG radiation for this enhancement to occur. This is obviously not the case for *a*-Si:H.

The hypothesis that EFISH has a limited contribution to the SHG response of *a*-Si:H films deposited on H terminated Si(100) provides important information on the surface passivation properties of the *a*-Si:H thin films. In general, surface passivation can be achieved by a reduction of recombination centers, typically surface defects, or by electrostatic shielding of charge carriers by internal electric fields, a phenomenon referred to as field-effect passivation. The observation that EFISH does not contribute significantly to the SHG response implies that the surface passivation mechanism of *c*-Si by *a*-Si:H thin films is not governed by field-effect passivation. The internal electric fields, caused, for example, by fixed charge, would result in a *c*-Si space-charge region and a significant EFISH contribution.[60] It can therefore be concluded that a reduction of recombination centers is dominating the surface passivation of *c*-Si by *a*-Si:H.[61–63] The increased H content in the *a*-Si:H in the interface region with the *c*-Si, as revealed by ATR-FTIR and TOF-SIMS, probably plays an important role in the passivation of defects at the *c*-Si surface, such as dangling bonds. Moreover, the conclusion that a reduction of recombination centers at the *c*-Si surface is the dominant *a*-Si:H passivation mechanism is also in agreement with the data presented in Fig. 1, where the formation of defect-rich epitaxial or mixed phase material strongly reduces the surface passivation properties at higher deposition temperatures.

D. Real-time second-harmonic generation

The SHG spectra demonstrate the sensitivity of the technique to the film/substrate interface and suggest that real-time SHG can provide more insight into the dynamics of the interface formation. In Fig. 14(a), the evolution of the SHG intensity at a SHG photon energy of 3.40 eV is shown during *a*-Si:H deposition on native oxide covered *c*-Si (film I). During the first ~60 s of film deposition, which corresponds to

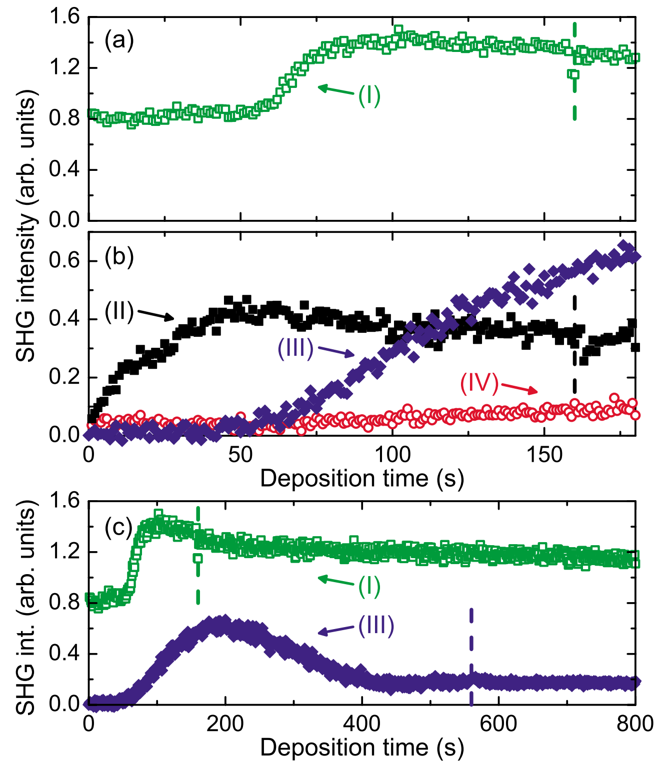

FIG. 14. (Color online) SHG intensity as a function of deposition time at a SHG photon energy of 3.40 eV and *pP* polarization for (a) *a*-Si:H deposited on native oxide covered Si(100) (film I) and (b) *a*-Si:H deposited on H terminated Si(100) (film II), *a*-Si:H with epitaxial onset of growth on H terminated Si(100) (film III), fully epi-Si deposited on H terminated Si(100) (film IV). In (c), the SHG intensity for *a*-Si:H on native oxide covered Si(100) (film I) and *a*-Si:H with epitaxial onset of growth on H terminated Si(100) (film III) is shown at a longer time scale. The deposition rate for films I–III was 34 Å/min and for film IV this was 21 Å/min. Dashed vertical lines indicate the termination of deposition.

~30 Å of film growth, the SHG intensity remains constant. After ~60 s, the SHG intensity rapidly increases, while after ~100 s of film deposition, the intensity decreases again. At 160 s, the film growth is terminated, however, the SHG intensity continues to decrease, as is also visible from Fig. 14(c) where the data are shown at a longer time scale. The time dependence of the SHG intensity during deposition on H terminated Si(100) substrates is shown in Fig. 14(b) for three different films. Films II and III were deposited on a substrate prepared by treatment A and film IV was deposited after treatment B. The SHG photon energy was again 3.40 eV, which is close to the E_0'/E_1 CP of *c*-Si and also corresponds to the minimum in the SHG spectrum for H terminated Si(100) at the deposition temperature of 150 °C (cf. Fig. 10). The SHG intensity for film II rapidly increases directly at the onset of deposition. The time scale of this increase and the magnitude of this increase are similar as observed for *a*-Si:H deposited on native oxide covered *c*-Si (film I). The SHG intensity for film II slowly decreases after ~50 s and remains constant after the film growth is terminated at 160 s. The intensity for film III remains nearly zero during the first ~50 s of film deposition. After this period of

~50 s, corresponding to ~20 Å of film growth, the intensity increases, however, not as rapidly as for film II. For increasing film thickness, the SHG intensity decreases again [Fig. 14(c)], which is in agreement with the decreasing trends for thicker films in the SHG spectra in Fig. 12. The SHG intensity does not change after terminating film growth at 560 s. The SHG intensity for film IV hardly changes and remains very low. Only a very slight increase is observed with increasing film thickness over a time frame of 180 s.

Real-time SE and ATR-FTIR experiments indicate that films II and III deposited on H terminated Si(100) are both amorphous, whereas the real-time SHG response of these films is significantly different. Cross sectional TEM confirms that film II developed fully amorphous with direct heterointerface formation, as shown in the high resolution TEM image in Fig. 15(a). However, as is visible from the high resolution TEM image in Fig. 15(b), the onset of growth for film III is epitaxial and is followed by rapid breakdown into mixed phase material after ~20 Å. Finally, the film continues to grow as purely amorphous material. Film IV, shown in Fig. 15(c), developed fully epitaxial during the deposition time in Fig. 14(b). For this film, the film/substrate interface can hardly be distinguished, except at some places where dislocation loops are visible. After ~250 Å, epitaxial breakdown into mixed phase material occurred, as visible from the growing cones of *a*-Si:H. The higher surface roughness observed with AFM after epitaxial breakdown is also visible from this TEM image. Figure 15(d) shows the TEM image for a mixed phase Si film, that is, a film that displayed epitaxial breakdown immediately at the onset of growth. This TEM image confirms the graded transition from epitaxial to amorphous material as found by SE, ATR-FTIR, and TOF-SIMS (cf. Fig. 5).

It can be concluded that differences in the initial film morphology strongly influence the real-time behavior of the SHG intensity for Si thin films deposited on H terminated Si(100). Deposition of epi-Si hardly affects the real-time SHG intensity, whereas the intensity rapidly increases once amorphous film growth sets in. The behavior for native oxide covered substrates is different; the initial SHG signal remains constant, while the onset of film growth is also directly amorphous (film I). This different behavior compared to the H terminated Si(100) substrates is most likely related to the difference in origin of the SHG signal. As concluded from the SHG spectra, the SHG signal for the native oxide covered substrates is governed by a contribution at the buried SiO_2/*c*-Si interface related to EFISH from the *c*-Si SCR, while the SHG signal for H terminated substrates consists of several comparable contributions from the surface. The first nucleation of amorphous material on the SiO_2 surface apparently has a limited influence on the SHG contribution from the buried interface.

The three real-time optical techniques as well as the *ex situ* diagnostics indicate a relation between film morphology and the two different substrate treatments for H terminated Si(100). Films deposited after substrate treatment A tend to develop amorphous with possibly some nanometer-level epitaxial material, while after treatment B, the probability to start the film growth epitaxially is higher resulting in mixed phase Si or even fully epitaxial Si. This difference might be related to surface roughness, as discussed in Sec. IV A. Both cleaning methods induce surface roughness on Si(100). However, after treatment B, a more structured roughness with larger scale local order and the appearance of (111) facets occurs.[52] A more ordered surface might explain the higher probability of epitaxial film growth after treatment B. In addition, the growth rate applied after treatment B is slightly lower, which likely also contributes to the higher

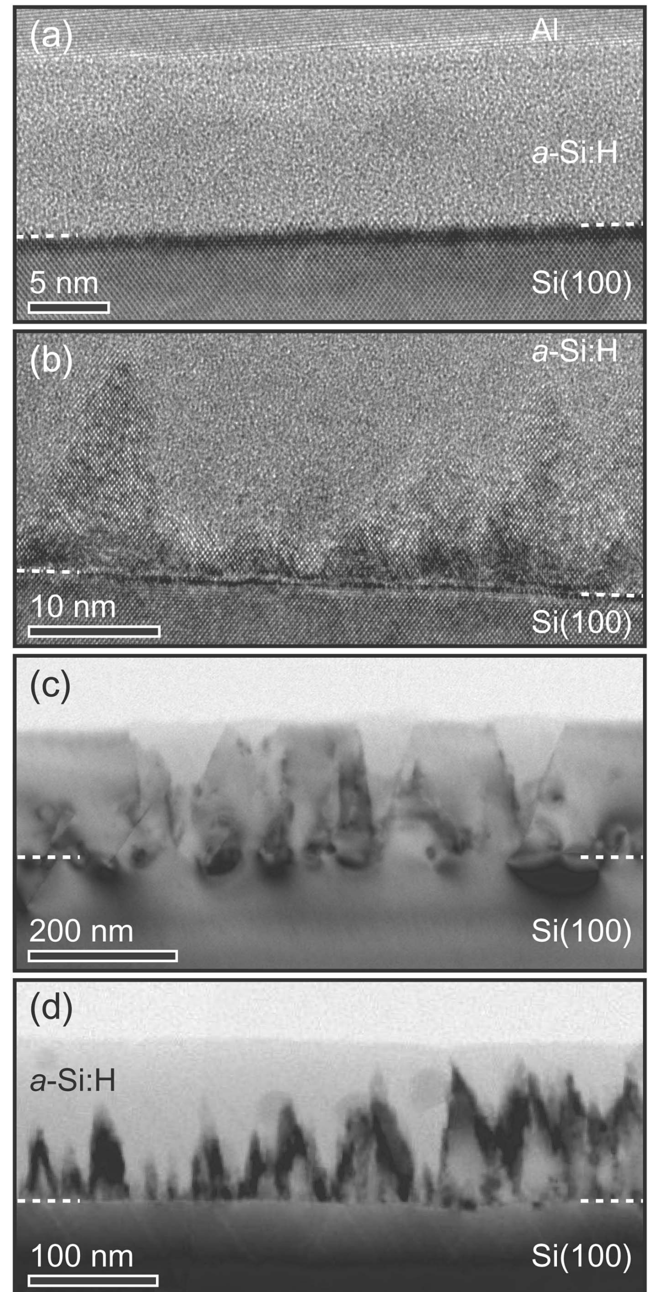

FIG. 15. Cross sectional TEM images for (a) *a*-Si:H deposited on H terminated Si(100), (b) *a*-Si:H with epitaxial onset of growth on H terminated Si(100), (c) fully epi-Si deposited on H terminated Si(100), and (d) mixed phase Si on H terminated Si(100). The dashed lines indicate the position of the interface between the films and the substrates. The images in (a)–(c) correspond to films II–IV in Fig. 14(b).

probability to form films with a higher crystalline fraction. A lower growth rate reduces the probability of forming crystallographic imperfections that induce epitaxial breakdown.[6,13,17]

V. CONCLUSIONS

The interface formation between Si thin films and native oxide covered Si(100) as well as H terminated Si(100) has been studied in real time during hot-wire chemical vapor deposition by using the three complementary optical techniques of SE, ATR-FTIR, and SHG. With SE and ATR-FTIR, the growth of amorphous, mixed phase, and epitaxial films has been detected. For mixed phase material, the *a*-Si:H content could be monitored, showing a gradual increase with film thickness. ATR-FTIR revealed a H-rich onset of film growth, especially for *a*-Si:H films. For ultrathin films (<20 Å), the sensitivity of SE and ATR-FTIR is limited due to low contrast between film and substrate and low initial absorbance, respectively. Real-time SHG, on the other hand, provides a method to distinguish between direct heterointerface formation, nanometer-level epitaxial growth and fully epitaxial growth at a very early stage of film growth. From spectroscopic SHG of *a*-Si:H on H terminated Si(100), it was concluded that the SHG signal is predominantly originating from the *c*-Si at the film/substrate interface, with an additional minor contribution from *a*-Si:H. In addition, the spectroscopic SHG results suggest that electric-field-induced SHG has a minor contribution to the total SHG response of *a*-Si:H on H terminated Si(100).

The results obtained by the three combined optical techniques indicate that the *c*-Si surface passivation properties of *a*-Si:H are not governed by field-effect passivation. Instead, it is plausible that *a*-Si:H films reduce the density of recombination centers at the *c*-Si surface. Direct measurement of these surface defects, for example, by applying SHG to probe Si dangling bonds, is an important subject for future investigation. The results reported have demonstrated that the simultaneous and real-time application of SE, ATR-FTIR, and SHG is a very valuable approach to monitor and control processes that occur during Si thin film growth. Especially the interface sensitive nature of SHG has a great potential to further increase the understanding of Si film growth; however, from the present work, it can also be inferred that for a well-founded interpretation of SHG studies, the combination with other (optical) methods is necessary.

ACKNOWLEDGMENTS

The authors thank M. J. F. van de Sande, J. F. C. Jansen, J. J. A. Zeebregts, and H. M. M. de Jong for their skillful technical assistance. R. F. Rumphorst is acknowledged for the design of the photon counting electronics in the SHG detection setup. This work was supported by the Netherlands Foundation for Fundamental Research on Matter (FOM). The research of W.K. has been made possible by the Royal Netherlands Academy of Arts and Sciences (KNAW).

*Corresponding author. Email address: w.m.m.kessels@tue.nl

[1] M. Taguchi, K. Kawamoto, S. Tsuge, T. Baba, H. Sakata, M. Morizane, K. Uchihashi, N. Nakamura, S. Kiyama, and O. Oota, Prog. Photovoltaics **8**, 503 (2000).

[2] S. Taira, Y. Yoshimine, T. Baba, M. Taguchi, H. Kanno, T. Kinoshita, H. Sakata, E. Maruyama, and M. Tanaka, in Proceedings of the 22nd European Photovoltaic Solar Energy Conference (2007), p. 932.

[3] M. Schaper, J. Schmidt, H. Plagwitz, and R. Brendel, Prog. Photovoltaics **13**, 381 (2005).

[4] I. Gordon, L. Carnel, D. Van Gestel, G. Beaucarne, and J. Poortmans, Prog. Photovoltaics **15**, 575 (2007).

[5] N. E. Posthuma, G. Flamand, W. Geens, and J. Poortmans, Sol. Energy Mater. Sol. Cells **88**, 37 (2005).

[6] D. J. Eaglesham, H.-J. Gossmann, and M. Cerullo, Phys. Rev. Lett. **65**, 1227 (1990).

[7] C. W. Teplin, D. H. Levi, E. Iwaniczko, K. M. Jones, J. D. Perkins, and H. M. Branz, J. Appl. Phys. **97**, 103536 (2005).

[8] S. Koveshnikov, W. Tsai, I. Ok, J. C. Lee, V. Torkanov, M. Yakimov, and S. Oktyabrsky, Appl. Phys. Lett. **88**, 022106 (2006).

[9] B. De Jaeger, R. Bonzom, F. Leys, O. Richard, J. Van Steenbergen, G. Winderickx, E. Van Moorhem, G. Raskin, F. Letertre, T. Billon, M. Meuris, and M. Heyns, Microelectron. Eng. **80**, 26 (2005).

[10] T. H. Wang, E. Iwaniczko, M. R. Page, D. H. Levi, Y. Yan, V. Yelundur, H. M. Branz, A. Rohatgi, and Q. Wang, in *Proceedings of the 31st IEEE Photovoltaic Specialists Conference* (IEEE, New York, 2005), p. 955; Y. Yan, M. Page, T. H. Wang, M. M. Al-Jassim, H. M. Branz, and Q. Wang, Appl. Phys. Lett. **88**, 121925 (2006).

[11] J. Schwarzkopf, B. Selle, W. Bohne, J. Röhrich, I. Sieber, and W. Fuhs, J. Appl. Phys. **93**, 5215 (2003).

[12] D. H. Levi, C. W. Teplin, E. Iwaniczko, T. H. Wang, and H. M. Branz, J. Vac. Sci. Technol. A **24**, 1676 (2006).

[13] H. Fujiwara and M. Kondo, Appl. Phys. Lett. **90**, 013503 (2007).

[14] R. A. Sinton and A. Cuevas, Appl. Phys. Lett. **69**, 2510 (1996).

[15] S. de Wolf and M. Kondo, Appl. Phys. Lett. **90**, 042111 (2007).

[16] S. de Wolf and G. Beaucarne, Appl. Phys. Lett. **88**, 022104 (2006).

[17] C. W. Teplin, Q. Wang, E. Iwaniczko, K. M. Jones, M. M. Al-Jassim, R. C. Reedy, and H. M. Branz, J. Cryst. Growth **287**, 414 (2006).

[18] H. C. Neitzert, W. Hirsch, and M. Kunst, Phys. Rev. B **47**, 4080 (1993); **48**, 4481 (1993).

[19] R. W. Collins and B. Y. Yang, J. Vac. Sci. Technol. B **7**, 1155 (1989).

[20] Y. M. Li, I. An, H. V. Nguyen, C. R. Wronski, and R. W. Collins, Phys. Rev. Lett. **68**, 2814 (1992).

[21] H. Fujiwara, Y. Toyoshima, M. Kondo, and A. Matsuda, Phys. Rev. B **60**, 13598 (1999).

[22] H. Fujiwara and M. Kondo, Appl. Phys. Lett. **86**, 032112 (2005).
[23] W. M. M. Kessels, J. P. M. Hoefnagels, E. Langereis, and M. C. M. van de Sanden, Thin Solid Films **501**, 88 (2006).
[24] P. J. van den Oever, M. C. M. van de Sanden, and W. M. M. Kessels, J. Appl. Phys. **101**, 123529 (2007).
[25] P. J. van den Oever, J. J. H. Gielis, M. C. M. van de Sanden, and W. M. M. Kessels, Thin Solid Films **516**, 511 (2008).
[26] J. J. H. Gielis, P. J. van den Oever, M. C. M. van de Sanden, and W. M. M. Kessels, Appl. Phys. Lett. **90**, 202108 (2007).
[27] D. C. Marra, E. A. Edelberg, R. L. Naone, and E. S. Aydil, J. Vac. Sci. Technol. A **16**, 3199 (1998).
[28] D. C. Marra, W. M. M. Kessels, M. C. M. van de Sanden, K. Kashefizadeh, and E. S. Aydil, Surf. Sci. **530**, 1 (2003).
[29] Y. R. Shen, *The Principles of Nonlinear Optics* (Wiley, New York, 1984).
[30] T. F. Heinz, *Second-order nonlinear optical effects at surfaces and interfaces*, in Nonlinear surface electromagnetic phenomena, edited by H. E. Ponath and G. I. Stegeman (Elsevier, Amsterdam, 1991), p. 353.
[31] W. M. M. Kessels, J. J. H. Gielis, I. M. P. Aarts, C. M. Leewis, and M. C. M. van de Sanden, Appl. Phys. Lett. **85**, 4049 (2004).
[32] G. Lüpke, Surf. Sci. Rep. **35**, 75 (1999).
[33] K. Pedersen and P. Morgen, Phys. Rev. B **52**, R2277 (1995); **53**, 9544 (1996).
[34] U. Höfer, Appl. Phys. A: Mater. Sci. Process. **63**, 533 (1996).
[35] T. Suzuki, Phys. Rev. B **61**, R5117 (2000).
[36] P. Lautenschlager, M. Garriga, L. Viña, and M. Cardona, Phys. Rev. B **36**, 4821 (1987).
[37] W. Daum, H.-J. Krause, U. Reichel, and H. Ibach, Phys. Rev. Lett. **71**, 1234 (1993).
[38] J. I. Dadap, Z. Xu, X. F. Hu, M. C. Downer, N. M. Russell, J. G. Ekerdt, and O. A. Aktsipetrov, Phys. Rev. B **56**, 13367 (1997).
[39] O. A. Aktsipetrov, A. A. Fedyanin, E. D. Mishina, A. N. Rubtsov, C. W. van Hasselt, M. A. C. Devillers, and Th. Rasing, Phys. Rev. B **54**, 1825 (1996).
[40] J. Bloch, J. G. Mihaychuk, and H. M. van Driel, Phys. Rev. Lett. **77**, 920 (1996).
[41] G. Erley and W. Daum, Phys. Rev. B **58**, R1734 (1998).
[42] A. Rumpel, B. Manschwetus, G. Lilienkamp, H. Schmidt, and W. Daum, Phys. Rev. B **74**, 081303(R) (2006).
[43] W. Daum, Appl. Phys. A: Mater. Sci. Process. **87**, 451 (2007).
[44] S. Alexandrova, P. Danesh, and I. A. Maslyanitsyn, Phys. Rev. B **61**, 11136 (2000).
[45] I. M. P. Aarts, J. J. H. Gielis, M. C. M. van de Sanden, and W. M. M. Kessels, Phys. Rev. B **73**, 045327 (2006).
[46] J. J. H. Gielis, P. M. Gevers, A. A. E. Stevens, H. C. W. Beijerinck, M. C. M. van de Sanden, and W. M. M. Kessels, Phys. Rev. B **74**, 165311 (2006).
[47] X. F. Hu, Z. Xu, D. Lim, M. C. Downer, P. S. Parkinson, B. Gong, G. Hess, and J. G. Ekerdt, Appl. Phys. Lett. **71**, 1376 (1997).
[48] W. Kern and D. A. Puotinen, RCA Rev. **31**, 187 (1970).
[49] E. C. Molenbroek, A. H. Mahan, and A. Gallagher, J. Appl. Phys. **82**, 1909 (1997).
[50] R. M. A. Azzam and N. M. Bashara, *Ellipsometry and Polarized Light* (North-Holland, Amsterdam, 1977).
[51] T. Yasuda and D. E. Aspnes, Appl. Opt. **33**, 7435 (1994).
[52] P. Dumas, Y. J. Chabal, and P. Jakob, Surf. Sci. **269/270**, 867 (1992).
[53] A. S. Ferlauto, G. M. Ferreira, J. M. Pearce, C. R. Wronski, R. W. Collins, X. Deng, and G. Ganguly, J. Appl. Phys. **92**, 2424 (2002).
[54] H. Fujiwara, J. Koh, P. I. Rovira, and R. W. Collins, Phys. Rev. B **61**, 10832 (2000).
[55] S. Kim and R. W. Collins, Appl. Phys. Lett. **67**, 3010 (1995).
[56] C. W. Teplin, E. Iwaniczko, B. To, H. Moutinho, P. Stradins, and H. M. Branz, Phys. Rev. B **74**, 235428 (2006).
[57] S. M. Han and E. S. Aydil, J. Vac. Sci. Technol. A **14**, 2062 (1996).
[58] A. H. M. Smets, W. M. M. Kessels, and M. C. M. van de Sanden, Appl. Phys. Lett. **82**, 1547 (2003).
[59] G. Erley, R. Butz, and W. Daum, Phys. Rev. B **59**, 2915 (1999).
[60] J. J. H. Gielis, B. Hoex, M. C. M. van de Sanden, and W. M. M. Kessels (unpublished).
[61] M. Garin, U. Rau, W. Brendle, I. Martin, and R. Alcubilla, J. Appl. Phys. **98**, 093711 (2005).
[62] S. Olibet, E. Vallat-Sauvain, and C. Ballif, Phys. Rev. B **76**, 035326 (2007).
[63] Field-effect passivation can be of influence when doped a-Si:H films are present in the system.